AGU ADVANCING EARTH AND SPACE SCIENCE

Geophysical Research Letters®

RESEARCH LETTER
10.1029/2022GL100799

Key Points:

- We estimate a time-averaged rate of strain transfer through block rotation in the Eastern Transverse Ranges to be between ~4.3 and 7.7 mm/yr
- New geologic slip rate points to a best fit variable slip rate, with a long-term average slip rate that agrees with regional kinematics
- The Blue Cut Fault presents another example of short-term strain rate variability being preserved in the geologic and geomorphic record

Supporting Information:

Supporting Information may be found in the online version of this article.

Correspondence to:

K. A. Guns,
kguns@ucsd.edu

Citation:

Guns, K. A., Bennett, R., Blisniuk, K., Walker, A., Hidy, A., & Heimsath, A. (2022). Steady long-term slip rate on the Blue Cut Fault: Implications for strain transfer between the San Andreas Fault and Eastern California Shear Zone. *Geophysical Research Letters*, *49*, e2022GL100799. https://doi.org/10.1029/2022GL100799

Received 11 AUG 2022
Accepted 29 SEP 2022

Author Contributions:

Conceptualization: K. A. Guns, R. Bennett, K. Blisniuk
Data curation: K. A. Guns, A. Walker, A. Hidy, A. Heimsath
Formal analysis: R. Bennett, A. Hidy, A. Heimsath
Funding acquisition: K. A. Guns, R. Bennett, K. Blisniuk, A. Heimsath
Investigation: K. A. Guns, K. Blisniuk, A. Walker
Methodology: K. Blisniuk, A. Walker, A. Hidy, A. Heimsath
Project Administration: K. A. Guns, R. Bennett, K. Blisniuk
Resources: K. Blisniuk
Supervision: R. Bennett, K. Blisniuk, A. Hidy, A. Heimsath

Steady Long-Term Slip Rate on the Blue Cut Fault: Implications for Strain Transfer Between the San Andreas Fault and Eastern California Shear Zone

K. A. Guns[1,2], R. Bennett[1,3], K. Blisniuk[4], A. Walker[4,5], A. Hidy[5], and A. Heimsath[6]

[1]Department of Geosciences, University of Arizona, Tucson, AZ, USA, [2]Now at Institute of Geophysics and Planetary Physics, Scripps Institution of Oceanography, University of California San Diego, La Jolla, CA, USA, [3]Now at NOAA-National Geodetic Survey, Silver Spring, MD, USA, [4]Department of Geology, San José State University, San Jose, CA, USA, [5]Lawrence Livermore National Laboratory, Center for Accelerator Mass Spectrometry, Livermore, CA, USA, [6]School of Earth and Space Exploration, Arizona State University, Tempe, AZ, USA

Abstract The Eastern Transverse Ranges (ETR) province of California contains a system of E-W-trending left-lateral faults accommodating clockwise block rotation between the San Andreas Fault (SAF) system in the Coachella Valley and the Eastern California Shear Zone (ECSZ) in the Mojave Desert. Building upon established geometric relationships, we estimate that this rotation across the ETR may transfer right-lateral strain from the SAF to the ECSZ at a time-averaged rate of ~4.3–7.7 mm/yr. Through geomorphic mapping and the analysis of 38 ^{10}Be surface exposure samples, we derive a long-term slip rate of 1.26 ± 0.50 (2$\boldsymbol{\sigma}$) mm/yr over the late Pleistocene, yet analysis of the displacement record indicates a rate decrease ~71 kya. While a rate change on this fault could have implications for possible plate boundary reorganization in this area, we argue that this slip rate variability more likely reflects routine fluctuation about a steady lifetime slip rate.

Plain Language Summary Neighboring zones of faulting within a tectonic plate boundary can play different roles in the accommodation and transfer of strain over time. Here, we investigate a zone of faulting that, in the past, has experienced clockwise block rotation, which can serve as a mechanism to communicate strain from one zone to another. We use previously published geometric relationships to determine that the Eastern Transverse Ranges (ETR) province may be transferring 4.3–7.7 mm/yr of strain from the San Andreas Fault zone to the Eastern California Shear Zone. In addition, using mapping and surface exposure geochronology, we estimate the slip-rate of a specific fault within the ETR to have a long-term rate of 1.26 ± 0.50 (2$\boldsymbol{\sigma}$) mm/yr over the late Pleistocene, with slight variation about that long-term rate, indicating that seismic hazard may vary over time.

1. Introduction

The San Andreas plate boundary fault system comprises dozens of faults that accommodate shearing between the Pacific and North America plates. Quantifying the time-dependent seismic hazards presented by this network is a major goal of active tectonics research and requires both a detailed accounting of slip recorded by the major throughgoing faults (e.g., the San Andreas Fault (SAF)), and an understanding of the roles played by subsidiary faults in the system. These secondary faults not only present their own seismic hazards, but may also affect the seismic hazard and earthquake potential of neighboring faults (e.g., Fletcher et al., 2016).

One of the most geometrically complex regions of the San Andreas plate boundary system lies northeast of Palm Springs, CA, where three zones of deformation connect: the SAF zone, the Eastern Transverse Ranges (ETR) province and the Eastern California Shear Zone (ECSZ). Slip accommodated by the Coachella Valley section of the SAF splits among three separate fault strands as it approaches the San Bernardino Mountains (Figure 1), while due east of the Coachella Valley the ETR comprises a series of E-W-trending left-lateral faults. Paleomagnetic data and palinspastic reconstructions suggest that these faults have accommodated 20–40° of clockwise block rotation over their <7 Ma lifetimes (Carter et al., 1987; Powell, 1993) in conjunction with slip on the SAF. In addition, the rotation of the ETR province has likely helped distribute localized right-lateral slip on the SAF system to the ECSZ, a zone of distributed, NW-trending, right-lateral faults in the Mojave Desert (Dickinson, 1996). The ECSZ has experienced strong recent seismicity, including three of the four M_W > 7.0 earthquakes to strike southern California in the last 50 years (i.e., the 1992 M_W 7.3 Landers, M_W 7.1 Hector Mine

Visualization: K. A. Guns, K. Blisniuk, A. Hidy
Writing – original draft: K. A. Guns
Writing – review & editing: K. A. Guns, R. Bennett, K. Blisniuk, A. Walker, A. Hidy, A. Heimsath

and the 2019 M_W 7.1 Ridgecrest events). Consequently, it has become an area of intense investigation to better understand the role of ECSZ faults in the broader plate boundary fault system. The faults of the ETR province serve as a pivotal pathway between the SAF and the ECSZ, and investigating the slip histories of these left-lateral faults will inform how these two zones may have communicated in recent time and how they may influence each other in the future.

This study investigates the slip history of the Blue Cut Fault (BCF) located in Joshua Tree National Park, one of the left-lateral faults that runs through the center of the modern ETR province (Figure 1). The BCF is part of a system of E-W-trending, throughgoing fault systems including, from north to south, the Pinto Mountain Fault (PMF), BCF, and Chiriaco Fault. The ETR province continues to the south with additional left-lateral faults that display Quaternary offsets, but not Pleistocene or Holocene age offsets. The PMF and the BCF are the two faults that currently experience microseismicity and show geomorphic evidence of modern faulting (Powell, 1993). The initiation age of these faults is constrained by K-Ar dating of offset volcanic formations to be 6–7 Ma, which is consistent in time with the formation of the Salton Trough and modern SAF strand in the region (5–6 Ma) (Langenheim & Powell, 2009). Langenheim and Powell (2009) conducted an analysis of block rotation along faults of the ETR by comparing recent geologic and geophysical data to show a cumulative left-lateral offset along all faults of 34–40 km, which corresponds to 27–39° of clockwise rotation accommodated over the last ~6 Ma. For the BCF, they estimate 3–6 km of offset along the west section and 7–10 km of offset along the east section, which, when combined with the estimated fault age of at least 5 Ma, provides a Ma-scale long-term slip rate of at most 1–2 mm/yr.

The BCF, along with the PMF to the north, have become recent centers of study due to their proximity to the large magnitude seismicity in 1992 (e.g., the M_W 6.1 Joshua Tree and M_W 7.3 Landers events)—in particular because the events did not rupture along these known left-lateral faults, but along a right-lateral, N-NW-trending fault plane cutting at a high angle to these faults. This unexpected activity sparked a debate about whether or not the PMF or BCF are in fact being replaced by a newly-forming fault system along the trend of the Eureka Peak Fault (i.e., the Landers-Mojave Earthquake Line of Nur et al., 1993). If the BCF is being bypassed by a newer, more kinematically efficient fault system, its most recent slip rates would likely fall below the long-term fault average. If, however, the most recent slip rates along the BCF are at or above the long-term fault average, this newer fault may either not be evolving as quickly, or may be evolving in conjunction with motion along the BCF. If we can determine the most recent fault slip record of the BCF, we can better inform possible hypotheses of future plate boundary evolution, in addition to improving seismic hazard estimates in this area. While there have been recent tectonic geomorphic studies of the PMF slip rate, the BCF represents a gap in our knowledge of most recent Pleistocene and Holocene slip history (Figure 1), and we set out here to remedy that gap.

Here, we focus our study the eastern end of a fault-controlled valley in the Hexie Mountains (Figure 1) where one to three strands of the BCF offset bedrock units composed of Pinto Gneiss and the Augen Gneiss of Monument Mountain (Powell et al., 2015) (Figure S1 in Supporting Information S1). This location features well preserved left-lateral offsets of geomorphic landforms, including debris flow and alluvial deposits and incised stream channels. We present results of our LiDAR- and field-based mapping, ^{10}Be surface exposure geochronology from six latest Pleistocene geomorphic surfaces and our slip rate calculations that document the slip rate history at our study site.

2. Methods

2.1. Tectonic Geomorphology

To document the slip rate history of the Hexie Mountains section of the BCF, we identify and estimate offsets of landforms using a combination of LiDAR- and field-based mapping efforts and constrain the ages of six offset surfaces using ^{10}Be cosmogenic radionuclide geochronology. To determine surface offsets, we first compile a geomorphic surface map (Figure 2). We use 1 m resolution LiDAR data to identify and map two sites, located 500 m apart from each other along the same section of the fault (Figure S1 in Supporting Information S1). We characterize seven total surfaces at these sites using relativistic qualitative surface attributes (e.g., levels of clast rubification and desert varnish, surface texture and color (Bull, 1991; McFadden et al., 1989)) and topographic data analysis (e.g., degree of dissection, orientation of incised streams (Frankel & Dolan, 2007)). Six of these surfaces are left-laterally offset and preserved on both sides of the fault, or can be correlated to their depositional

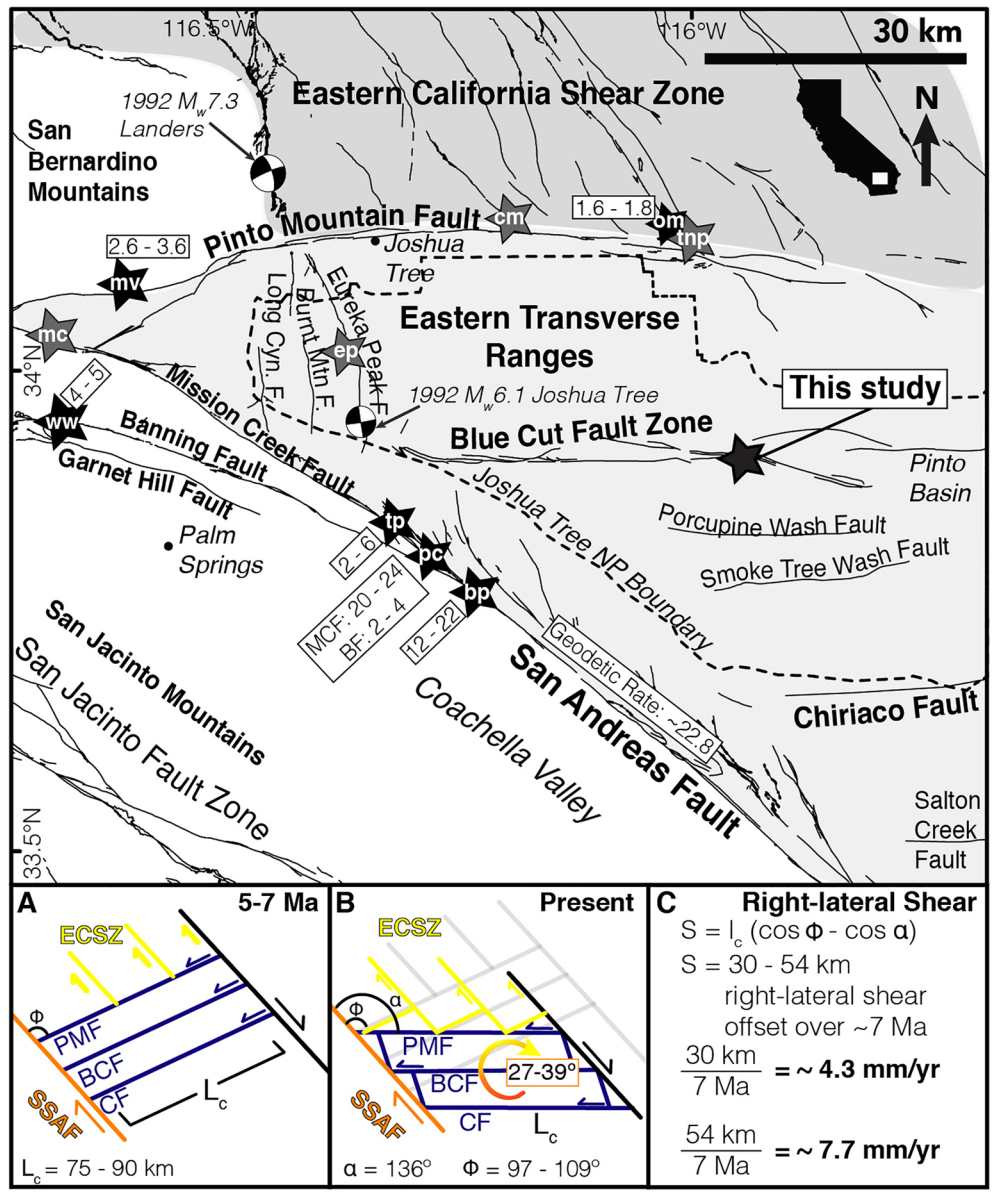

Figure 1. Regional fault map of Eastern Transverse Ranges (ETR) province; faults in the ETR have accommodated clockwise block rotation over the last ~5–7 Ma; (a) shows past configuration of ETR faults, (b) shows the rotated, modern-day version; (c) shows the calculation of the transfer of right-lateral shear from the San Andreas Fault (SAF) to the Eastern California Shear Zone (ECSZ) using the equations of Dickinson (1996), and an estimated rate of transferred shear assuming constant rotation through time. Slip rates are reported in mm/yr at sites bp = Biskra Palms (Behr et al., 2010), ep = Eureka Peak (Hislop, 2019), mv = Morongo Valley (Gabriel, 2017), om = Oasis of Mara (Cadena, 2013), pc = Pushawalla Canyon (Blisniuk et al., 2021), tp = Thousand Palms (Fumal et al., 2002), ww = Whitewater (Gold et al., 2015). Active study sites are cm = Copper Mountain (Dudash, 2019), mc = Mission Creek (Waco & Blisniuk, 2019), and tnp = Twentynine Palms (Menges & Dudash, 2019). Focal mechanisms from the USGS earthquake catalog.

source (Figure 2; Table 1; see Table S1 in Supporting Information S1 for list of offset landforms). We reconstruct correlated surfaces to determine minimum and maximum estimates of fault offset (Figures S2–S7 in Supporting Information S1), and assemble a geomorphic evolution explanation of each site (Figures S8 and S9 in Supporting Information S1). We conservatively include all possible offsets in our reconstructions; in general our minimum reconstructions are channels incised into their give deposit. These are minimum offsets because incision by the channels must have occurred during the emplacement of, or after deposition of the surface. Maximum reconstructions reunite edges of mapped surface deposits across the fault. In both sites we encounter areas where younger

10.1029/2022GL100799

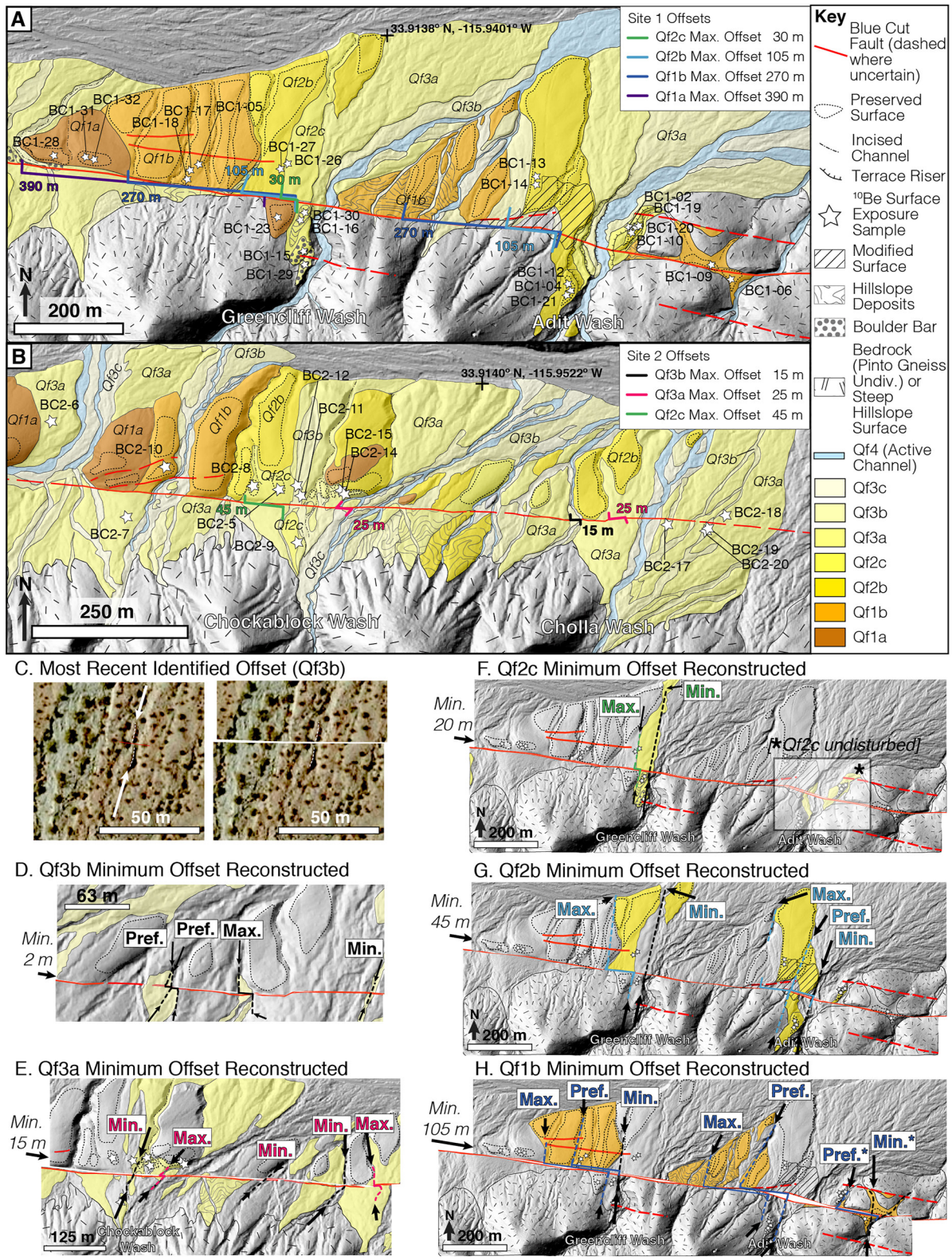

Figure 2. Final geomorphic surface map and reconstructions of our two study sites along the Blue Cut Fault (BCF), with plotted maximum landform offsets and ^{10}Be sample locations; (a) is Site 1, located 500 m to the east of (b) Site 2. Note change in scale between sites; (c–h) show isolated individual surfaces, reconstructed to their minimum offset values, with marked landforms with minimum, maximum, or preferred offsets (See Figures S2–S7 in Supporting Information S1 for additional reconstruction details).

Table 1
Surface Age, Offset, and Slip Rate Results

Surface	Number of ^{10}Be samples	Boxcar surface age[a] (ka) ± (2σ)	ISOPLOT surface age[b] (ka) ± (2σ)	Min/max offsets (m) mean ± min/max	Preferred offset[c] (m)	Single long-term rate[d] (mm/yr) ± (2σ)	One change in rate[d] (younger) (mm/yr) ± (2σ)	One change in rate[d] (older) (mm/yr) ± (median, 95%CI)
Qf3b	4	13.3 ± 2	13.2 ± 1	9 ± 7	7 ± 2	Using Min/Max Offsets =	–	–
Qf3a	6	24.3 ± 8	21.9 ± 2	20 ± 5	N/A[e]	1.26 ± 0.50	0.66 ± 0.20[f]	2.93 + 6.14/−1.98
Qf2c	8	57.0 ± 10	55.5 ± 3	33 ± 12	N/A[e]		–	–
Qf2b	5	81.1 ± 15	80.9 ± 7	75 ± 30	90 ± 3	Using Preferred Offsets =	–	–
Qf1b	5	121 ± 30	119 ± 10	188 ± 83	240 ± 5	1.56 ± 0.16	0.64 ± 0.30[g]	4.09 + 3.59/−1.91
Qf1a[h]	4	>121 ± 30	>119 ± 10	330 ± 60	355 ± 5		–	–

[a]Calculated using MATLAB-based Slip Rate Tools created by Zechar and Frankel (2009). [b]Calculated using ISOPLOT (Vermeesch, 2018). [c]Preferred offset uncertainty calculated as half the width of the reconstructed offset channel (Figures S2–S7 in Supporting Information S1). [d]Calculated using the Slip Rate Calculator (Styron, 2015), using ISOPLOT-calculated ages. [e]Preferred offset not constrained. [f]Rate change calculated at 71 ± 15 ka (1σ) from Slip Rate Calculator (Styron, 2015). [g]Rate change calculated at 69 ± 11 ka (1σ) from Slip Rate Calculator (Styron, 2015). [h]Surface age not used in overall slip rate calculation due to lack of well-constrained age.

surfaces have been deposited atop, or have reworked older surfaces. These appear to occur after the deposition of surface Qf2b, perhaps indicating a possible deceleration in slip rate around this time.

2.2. ^{10}Be Cosmogenic Surface Exposure Dating

To constrain the timing of deposition of these offset geomorphic landforms, we apply ^{10}Be exposure dating, which has been frequently used to date the arid landscapes of southern California (e.g., Blisniuk et al., 2021; Heermance & Yule, 2017; Owen et al., 2014). To mitigate the effects of potential exhumation and inheritance, processes that can skew exposure ages younger or older, respectively, we collected multiple sample types from each surface, including boulder-tops, cobbles, and amalgamated pebble samples (at least two types, with all three types in four of seven dated surfaces). Age agreement between sample types indicates that effects of these processes are negligible, because sample types are differentially affected by inheritance/exhumation. Seven of our total 38 samples were processed at Arizona State University, while the rest were processed jointly at San José State University and Lawrence Livermore National Laboratory, following the procedures of Ditchburn and Whitehead (1994). We calculate final ^{10}Be model ages using Version 3 of the exposure age calculator described in Balco et al. (2008) (Table S2). To calculate overall ages for each surface we use both the web-based IsoPlot program (Vermeesch, 2018) and the MATLAB-based slip rate tools (Zechar & Frankel, 2009) (Table 1; see Table S3 in Supporting Information S1 for sample ages organized by surface). We also plot normalized kernel density estimate curves for each surface (Figure S10 in Supporting Information S1).

2.3. Geologic Slip Rate and Strain Transfer Calculations

To calculate slip rates, we use the Python-based Slip Rate Calculator (Styron, 2015), which uses Monte Carlo sampling (n = 10,000) from a probability density function for the age and offset of a given landform and fits a linear regression to the sample data point. We calculate slip rates using a conservative boxcar approach for offsets, and a Gaussian approach for surface ages, wherein we use the IsoPlot-calculated ages and uncertainties. In the case of a non-Gaussian distribution of slip rate, we estimate a 95% confidence interval to describe the uncertainties (Figure S11 in Supporting Information S1).

The geometric relationships between rotating crustal blocks has been described by many authors in various areas of the globe (e.g., Nur et al., 1986; Ron et al., 1984), including the ETR region (e.g., Carter et al., 1987; Dickinson, 1996; Powell, 1993). We employ the equations and analysis of Dickinson (1996) to determine a fault-lifetime rate of shear transfer between the SAF and the ECSZ through rotation in the ETR. Dickinson (1996) posits two possible scenarios of transferred right-lateral shear, different due to the uneven mapped block lengths (L_c of either 75 or 90 km in Figure 1a) of the ETR blocks. Where he assumes a fault-lifetime clockwise block rotation of ~44° in both cases, we apply a range of 27–39° of clockwise rotation, derived by Langenheim and

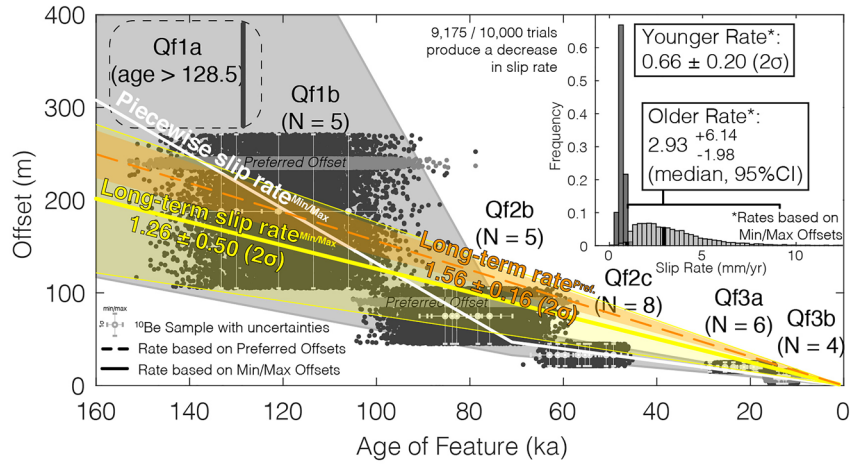

Figure 3. Plot of Monte Carlo slip rate calculation trials from a boxcar range of measured offsets and a Gaussian distribution of surface ages (Table 1); This illustrates both a best-fit 100-ka-scale long-term slip rate using min/max offsets (yellow line with uncertainty shadow) and preferred offsets (orange dashed line and uncertainty shadow) and a best-fit time-variable slip rate (white line, with gray uncertainty shadow using min/max offsets). White circles with error bars show individual sample ages plotted with min/max offsets. Inset shows the distributions of the younger and older slip rate trial values (upper right).

Powell (2009), in order to calculate an updated range of estimated right lateral shear. We then build upon the analysis of Langenheim and Powell (2009) and Dickinson (1996) by dividing the estimated transferred right lateral shear of 30–54 km by the approximate lifetime of fault motion, and determining that (assuming constant block rotation over 7 ma), this package of rotating blocks could transfer 4.3–7.7 mm/yr of shear from the SAF in the northern Coachella Valley to the ECSZ.

3. Results

^{10}Be geochronological results, in combination with geomorphic mapping indicate multiple ages of offset alluvial surfaces that range from the oldest mapped Qf1a surface of >129 ka, to the youngest offset Qf3b surface of 13.2 ± 1 ka (2**σ**) (Table 1). In addition, we find good agreement between ages of different sample types for each surface (Table S3 in Supporting Information S1). Figure 2 presents our final mapping interpretation for both sites, along with surface offset reconstructions. We find that the combination of minimum/maximum offsets and calculated surface ages along the BCF produces a best fit piecewise slip rate of 2.93 + 6.14/−1.98 (median, 95% CI) mm/yr before 71 ± 15 (1**σ**) ka and a best fit slip rate of 0.66 ± 0.20 (2**σ**) mm/yr after (Figure 3). The age of slip rate decrease, and its uncertainty range is solved for during the regression process. When we fit a single long term slip rate, this data produces a rate of 1.26 ± 0.50 (2**σ**) mm/yr (1.56 ± 0.16 (2**σ**) when using preferred offsets). We have not attempted to quantify any amount of off-fault deformation in this study area, and because we assume zero erosion rate exposure ages for our samples, these slip rates reflect minimum slip rates on the main strand of the fault.

4. Discussion

While a decrease in apparent slip rate along a fault can imply regional changes in strain accumulation and fault organization, we argue that the BCF is more likely maintaining its Ma-scale long-term slip rate of 1–2 mm/yr for three main reasons: (a) the Ma-scale slip rates of the BCF, as determined by geologic and geophysical offsets (Langenheim & Powell, 2009), match our 100 ka-scale long-term rate, (b) time-averaged block rotation calculations (Dickinson, 1996) produce consistent transferred right-lateral shear to the cumulative slip rates of the ECSZ, an area of modern seismic activity, and (c) observed "slip rate variability" can reflect natural fluctuations in earthquake recurrence intervals that average to a secular slip rate over sufficiently long periods of time (e.g., Friedrich et al., 2003).

First, our estimated 100 ka-scale long-term fault slip rate agrees with the rate determined from the cumulative geologic and/or geophysical offsets along the BCF. Langenheim and Powell (2009) calculate the present-day

offsets between lithologic units and magnetic anomalies measured along these faults and show that the eastern section of the BCF has accommodated 7–10 km of offset over the past 5–7 Ma indicating a Ma-scale time-averaged slip rate of 1–2 mm/yr. This matches our estimated 100 ka-scale rate of 1.26 mm/yr. Neither our older or younger time-variable slip rates can produce a similar total offset in that time span. Our best-fit older rate of 2.93 mm/yr produces ∼15–21 km total offset, while our best-fit younger rate of 0.66 mm/yr produces ∼3–5 km total offset. This suggests that while variability can appear in the slip rate record, cumulative offsets are best explained by the long-term rate.

Second, when we estimate the overall right-lateral shear transferred by the ETR faults over their 5–7 Ma lifetimes using previously published rotation estimates, we find that this system alone could have transferred at least 4.3–7.7 mm/yr of right-lateral strain from the SAF to the ECSZ (Figures 1a–1c), assuming a constant block rotation rate through time. These values correspond intriguingly well to the 4.3–8.1 mm/yr cumulative slip rates estimated by Oskin et al. (2008) across the faults of the ECSZ in the Mojave Desert. Such consistency could indicate that block rotation in the ETR continues to feed strain into the ECSZ from the SAF, in the same way it has in the past. Any disruption of this steady conveyance of strain would have consequences for activity in the ECSZ, implying that earthquake clustering in the ECSZ (e.g., Rockwell et al., 2000) may also maintain a steady long-term average.

Third, the observation that apparent slip rate can vary within the time window of paleoseismic and geomorphic investigation is not unique. Friedrich et al. (2003) found that Holocene slip rates on the Wasatch Fault could exceed longer-term 100 ka-time scale rates due to clustering of seismic activity on a 10 ka-time scale ("Wallace-type" behavior; i.e., Wallace (1987)). In southern California, Weldon et al. (2004) also observe apparent slip rate changes from a paleoseismic record along the SAF, with slip rate within a cluster of earthquakes jumping to 89 mm/yr, while the long-term rate averages to 31 mm/yr. Examples along the Garlock (e.g., Dolan et al., 2016; Rittase et al., 2014), White Mountain (e.g., Kirby et al., 2006) and San Jacinto (e.g., Kendrick et al., 2002; Sharp, 1981) faults also exhibit a similar kind of temporal variability of slip rate. Changes in rate may be due to the random variability of stress buildup or fault frictional resistance leading to an irregular pattern of seismic release. In the case of southern California, the hypothesis put forth by Dolan et al. (2007) posits that cycles of increased seismic activity switch between the SAF and the ECSZ. With the ETR province placed in between the two, any cyclic activity observed along faults of the ETR could be evidence of a link between the two larger zones. Since, however, the most recently offset surface along the BCF is ∼13 ka old, and there is a younger undisturbed surface of <12 ka Holocene age, that would indicate that no surface rupturing events have occurred along the BCF since then, while several cycles of activity have occurred between the ECSZ and SAF (Dolan et al., 2007).

A fault capable of variable strain release through periods of increased or decreased earthquake activity over time would, however, experience time-dependent seismic hazard. Though we can only speculate on when and how these changes could occur in the future, the most recently observed minimum surface offset of 2 m (for surface Qf3b; see Figure S2 in Supporting Information S1), would require the occurrence of one $\sim M_W$7.2 to five $\sim M_W$6.0 events (calculated using the relationships of Wells and Coppersmith (1994) (Table S4 in Supporting Information S1)). If significant off-fault deformation occurs during events on this fault, however, these magnitudes could be underestimated (Milliner et al., 2016). The fact that we can measure large surface displacements implies that surface-rupturing earthquake events have occurred in the past, and could occur in the future, in the absence of surface creep.

The result that the BCF has recorded a slower slip rate in the recent past can also support an alternative conclusion: that the BCF, and potentially block rotation, is coming to a halt. This observation fits with the recent increased activity of the Eureka Peak Fault, which likely hosted the M_w 6.1 Joshua Tree earthquake in 1992, and potentially two other Holocene events (Rymer, 2000). The Eureka Peak Fault could serve as a new, and more direct, avenue of strain transfer between the SAF and the ECSZ, thereby replacing the need for a system of block-rotating faults like the ETR system (Hislop, 2019; Nur et al., 1993). Moreover, since the throughgoing left-lateral faults south of the BCF (e.g., the Chiriaco Fault, the Salton Creek Fault) have experienced less and less activity over time (to the point where there is little to no Late Pleistocene or Holocene slip recorded, nor active microseismicity), the BCF may be next in line for a slow-down or halt. The timescales on which plate boundaries reorganize, however, suggests that while this hypothesis is certainly possible, more investigation (and time) is required evaluate it.

5. Conclusions

The BCF in the ETR province is part of a zone of faults that kinematically links strain from the SAF system to the ECSZ, and may be conveying 4.4–7.3 mm/yr of strain from one system to the other. By characterizing its slip rate chronology over the late Pleistocene, through detailed geomorphic mapping and ^{10}Be surface exposure dating analyses, we have documented a best fit long-term slip rate of 1.26 ± 0.50 (2$\boldsymbol{\sigma}$) mm/yr. Our calculated long-term rate is consistent with the Ma-scale regional behavior of block rotation, and is in good agreement with the time-averaged rate of 1–2 mm/yr previously derived from cumulative geologic and geophysical offsets. We argue that the apparent slip rate variability we observe at this site is most likely due to natural fluctuations in strain released by earthquakes over time, and that the BCF is likely capable of hosting surface-rupturing events of ~M_W 6.0–7.2 in the future.

Data Availability Statement

All LiDAR elevation data presented and used within this analysis is freely available on OpenTopography.org (see data set "Slip transfer through the Eastern Transverse Ranges, CA 2017": https://doi.org/10.5069/G9D21VP1). All geochronological data presented and used within this analysis is available within the EarthChem Library (Guns et al., 2022; https://doi.org/10.26022/IEDA/112685) and available in Supporting Information S1. All software used to process our geochronological and offset measurement data is freely available; Version 3 of the exposure age calculator is described by Balco et al. (2008) and freely available at https://hess.ess.washington.edu/ using the "Calculate exposure age" option; We use the MATLAB-based code camelplot.m, written by Greg Balco and available here: http://depts.washington.edu/cosmolab/pubs/gb_pubs/camelplot.m; MATLAB-based Slip Rate Tools is described and available within the Supporting Information of Zechar and Frankel (2009), while the Python-based Slip Rate Calculator is available on GitHub (https://github.com/cossatot/slip_rate_calculator) and cited as Styron (2015).

Acknowledgments
The authors thank James Spotila and an anonymous reviewer for their feedback that greatly improved the presentation of this work. The authors also thank Luke Sabala and Jay Theuer from the National Park Service for their support in obtaining a scientific research permit for Joshua Tree National Park. The collection of samples was partially funded by GSA Graduate Student Research Grant awards to K. Guns and Southern California Earthquake Center Grant 17161. Sample processing was funded by the EarthScope AGeS Program, USGS NEHRP Award G19AP00054 and NSF Early Career Award 1848547 to K. Blisniuk. Prepared in part by LLNL under Contract DE-AC52-07NA27344. This is LLNL-JRNL-826988.

References

Balco, G., Stone, J. O., Lifton, N. A., & Dunai, T. J. (2008). A complete and easily accessible means of calculating surface exposure ages or erosion rates from ^{10}Be and ^{26}Al measurements. *Quaternary Geology*, *3*, 174–195. https://doi.org/10.1016/j.quageo.2007.12.001

Behr, W. M., Rood, D. H., Fletcher, K. E., Guzman, N., Finkel, R., Hanks, T. C., et al. (2010). Uncertainties in slip-rate estimates for the mission creek strand of the southern San Andreas Fault at Biskra Palms Oasis, southern California. *The Geological Society of America Bulletin*, *122*(9–10), 1360–1377. https://doi.org/10.1130/B30020.1

Blisniuk, K., Scharer, K., Sharp, W. D., Bürgmann, R., Amos, C., & Rymer, M. (2021). A revised position for the primary strand of the Pleistocene-Holocene San Andreas fault in southern California. *Science Advances*, *7*(13), eaaz5691. https://doi.org/10.1126/sciadv.aaz5691

Bull, W. B. (1991). *Geomorphic responses to climate change*. Oxford University Press.

Cadena, A. M. (2013). *Paleoseismologic evidence for Holocene activity on the Pinto Mountain Fault, Twentynine Palms* (M. S. Thesis). Central Washington University. Retrieved from https://digitalcommons.cwu.edu/etd/1448/

Carter, J. N., Luyendyk, B. P., & Terres, R. R. (1987). Neogene clockwise tectonic rotation of the eastern Transverse Ranges, California, suggested by paleomagnetic vectors. *GSA Bulletin*, *98*(2), 199–206. https://doi.org/10.1130/0016-7606(1987)98<199:nctrot>2.0.co;2

Dickinson, W. R. (1996). *Kinematics of transrotational tectonism in the California transverse ranges and its contribution to cumulative slip along the San Andreas transform fault system*. Geological Society of America Special.Paper 305.

Ditchburn, R. G., & Whitehead, N. E. (1994). The separation of ^{10}Be from silicates: 3D workshop of the south pacific environmental radioactivity association (pp. 4–7).

Dolan, J. F., Bowman, D. D., & Sammis, C. G. (2007). Long-range and long-term fault interactions in Southern California. *Geology*, *35*(9), 855–858. https://doi.org/10.1130/G237889A.1

Dolan, J. F., McAuliffe, L. J., Rhodes, E. J., McGill, S. F., & Zinke, R. (2016). Extreme multi-millennial slip rate variations on the Garlock fault, California: Strain super-cycles, potentially time-variable fault strength, and implications for system-level earthquake occurrence. *Earth and Planetary Science Letters*, *446*, 123–136. https://doi.org/10.1016/j.epsl.2016.04.011

Dudash, S. L. (2019). *Initial mapping along the central reach of the Pinto Mountain Fault Zone, southern California, reveals new insights into tectonics and paleohydrography*. Geological Society of America Abstracts with Programs. https://doi.org/10.1130/abs/2019AM-342032

Fletcher, J. M., Oskin, M. E., & Teran, O. J. (2016). The role of a keystone fault in triggering the complex El Mayor-Cucapah earthquake rupture. *Nature Geoscience*, *9*(4), 303–307. https://doi.org/10.1038/NGEO2660

Frankel, K. L., & Dolan, J. F. (2007). Characterizing arid region alluvial fan surface roughness with airborne laser swath mapping digital topographic data. *Journal of Geophysical Research*, *112*(F2), F02025. https://doi.org/10.1029/2006JF000644

Friedrich, A. M., Wernicke, B. P., Niemi, N. A., Bennett, R. A., & Davis, J. L. (2003). Comparison of geodetic and geologic data from the Wasatch region, Utah, and implications for the spectral character of Earth deformation at periods of 10 to 10 million years. *Journal of Geophysical Research*, *108*(B4), 2199. https://doi.org/10.1029/2001JB000682

Fumal, T. E., Rymer, M. J., & Seitz, G. G. (2002). Timing of large earthquakes since A.D. 800 on the mission creek strand of the San Andreas fault zone at thousand palms oasis, near Palm Springs, California. *Bulletin of the Seismological Society of America*, *92*(7), 2841–2860. https://doi.org/10.1785/0120000609

Gabriel, K. (2017). Late Pleistocene slip rate for the Western Pinto Mountain Fault, Morongo Valley, southern California (Ph.D Dissertation). *Scholar Works*. https://scholarworks.csun.edu/handle/10211.3/195491

Gold, P. O., Behr, W. M., Rood, D., Kendrick, K., Rockwell, T. K., Sharp, W. D., & Salin, A. (2015). Holocene geologic slip rate for the banning strand of the southern San Andreas Fault, southern California. *Journal of Geophysical Research: Solid Earth*, *120*(8), 5639–5663. https://doi.org/10.1002/2015JB012004

Guns, K. A., Bennett, R., Blisniuk, K., Walker, A., Hidy, A., & Heimsath, A. (2022). 10-Be surface exposure ages along the blue cut fault in Joshua Tree National Park, California, Version 1.0 [Dataset]. Interdisciplinary Earth Data Alliance (IEDA). https://doi.org/10.26022/IEDA/112685

Heermance, R. V., & Yule, D. (2017). Holocene slip rates along the san Andreas Fault system in the san gorgonio pass and implications for large earthquakes in southern California. *Geophysical Research Letters*, *44*(11), 5391–5400. https://doi.org/10.1002/2017GL072612

Hislop, A. (2019). Fault evolution in the northwest little san Bernardino Mountains, southern California: A reflection of tectonic linkage between the san Andreas Fault and the eastern California shear zone (Ph.D. Dissertation). *UKnowlegde Dissertation Repository*. https://uknowledge.uky.edu/ees_etds/63/

Kendrick, K. J., Morton, D. M., Wells, S. G., & Simpson, R. W. (2002). Spatial and temporal deformation along the northern san Jacinto fault, southern California: Implications for slip rates. *Bulletin of the Seismological Society of America*, *92*(7), 2782–2802. https://doi.org/10.1785/0120000615

Kirby, E., Burbank, D. W., Reheis, M., & Phillips, F. (2006). Temporal variations in slip rate of the white Mountains Fault zone, eastern California. *Earth and Planetary Science Letters*, *248*(1–2), 168–185. https://doi.org/10.1016/j.epsl.2006.05.026

Langenheim, V. E., & Powell, R. E. (2009). Basin geometry and cumulative offsets in the Eastern Transverse Ranges, southern California: Implications for transrotational deformation along the San Andreas fault system. *Geosphere*, *5*(1), 1–22. https://doi.org/10.1130/GES00177.1

McFadden, L. D., Ritter, J. B., & Wells, S. B. (1989). Use of multiparameter relative-age methods for age estimation and correlation of alluvial fan surfaces on a desert piedmont, eastern Mojave Desert, California. *Quaternary Research*, *32*(3), 276–290. https://doi.org/10.1016/0033-5894(89)90094-x

Menges, C. M. & Dudash, S. L. (2019). Relative Patterns of Neotectonic Deformation along the Eastern Garlock and Eastern Pinto Mountain Fault Zones: Two Domain-Bounding Transverse Structures within the Eastern California Shear Zone. *Geological Society of America Abstracts with Programs*. https://doi.org/10.1130/abs/2019AM-340629

Milliner, C. W. D., Dolan, J. F., Hollingsworth, J., Leprince, S., & Ayoub, F. (2016). Comparison of coseismic near-field and off-fault surface deformation patterns of the 1992 MW 7.3 Landers and 1999 MW 7.1 Hector Mine earthquakes: Implications for controls on the distribution of surface strain. *Geophysical Research Letters*, *43*(19), 10115–10124. https://doi.org/10.1002/2016GL069841

Nur, A., Ron, H., & Beroza, G. C. (1993). The nature of the Landers-Mojave earthquake Line. *Science*, *261*(5118), 201–203. https://doi.org/10.1126/science.261.5118.201

Nur, A., Ron, H., & Scotti, O. (1986). Fault mechanics and the kinematics of block rotations. *Geology*, *14*(9), 746–749. https://doi.org/10.1130/0091-7613(1986)14<746:fmatko>2.0.co;2

Oskin, M., Perg, L., Shelef, E., Strane, M., Gurney, E., Singer, B., & Zhang, X. (2008). Elevated shear zone loading rate during an earthquake cluster in eastern California. *Geology*, *36*(6), 507–510. https://doi.org/10.1130/G24814A.1

Owen, L. A., Clemmens, S. J., Finkel, R. C., & Gray, H. (2014). Late quaternary alluvial fans at the eastern end of the san Bernardino Mountains, southern California. *Quaternary Science Reviews*, *87*, 114–134. https://doi.org/10.1016/j.quascirev.2014.01.003

Powell, R. E. (1993). Balanced palinspastic reconstruction of pre-late Cenozoic paleogeogeology, southern California: Geologic and kinematic constraints on evolution of the San Andreas fault system. In R. E. Powell, R. J. Weldon, & J. C. Matti (Eds.), *The San Andreas fault system: Displacement, palinspastic reconstruction, and geologic evolution: Boulder, Colorado* (Vol. 178). Geological Society of America Memoir.

Powell, R. E., Matti, J. C., & Cossette, P. M. (2015). Geology of Joshua tree national Park geodatabase. Report 2015-1175. *USGS*. https://doi.org/10.3133/ofr20151175

Rittase, W. M., Kirby, E., McDonald, E., Walker, J. D., Gosse, J., Spencer, J. Q. G., & Herrs, A. J. (2014). Temporal variations in Holocene slip rate along the central Garlock fault, pilot knob valley, California. *Lithosphere*, *6*(1), 48–58. https://doi.org/10.1130/L286.1

Rockwell, T., Lindvall, S., Herzberg, M., Murbach, D., Dawson, T., & Berger, G. (2000). Paleoseismology of the Johnson valley, kickapoo, and homestead valley faults: Clustering of earthquakes in the eastern California shear zone. *Bulletin of the Seismological Society of America*, *90*(5), 1200–1236. https://doi.org/10.1785/0119990023

Ron, H., Freund, R., Garfunkel, Z., & Nur, A. (1984). Block rotation by strike-slip faulting: Structural and paleomagnetic evidence. *Journal of Geophysical Research*, *89*(B7), 6256–6270. https://doi.org/10.1029/jb089ib07p06256

Rymer, M. J. (2000). Triggered surface slips in the Coachella Valley area associated with the 1992 Joshua tree and Landers, California, earthquakes. *Bulletin of the Seismological Society of America*, *90*(4), 832–848. https://doi.org/10.1785/0119980130

Sharp, R. V. (1981). Variable rates of late quaternary strike slip on the San Jacinto Fault Zone, southern California. *Journal of Geophysical Research*, *86*(B3), 1754–1762. https://doi.org/10.1029/JB086iB03p01754

Styron, R. (2015). Slip rate calculator v.0.1.2: A program for calculating fault slip rates from inputs of surface age and fault offset. *Zenodo*. https://doi.org/10.5281/zenodo.33360

Vermeesch, P. (2018). IsoplotR: A free and open toolbox for geochronology. *Geoscience Frontiers*, *9*(5), 1479–1493. https://doi.org/10.1016/j.gsf.2018.04.001

Waco, J., Blisniuk, K., Chen, Z., Scott, C. P., & Das, J. (2019). Geologic map from mission creek preserve to whitewater river, san Bernardino and riverside counties, California: Evidence for an active and evolving left-stepping san Andreas Fault (mission creek strand) in the eastern san Bernardino Mountains. *Geological Society of America Abstracts with Programs*, *51*(5), 340878. https://doi.org/10.1130/abs/2019AM-340878

Wallace, R. E. (1987). Grouping and Migration of surface faulting and variations in slip rates on faults in the Great Basin Province. *Bulletin of the Seismological Society of America*, *77*(3), 868–876.

Weldon, R., Scharer, K., Fumal, T., & Biasi, G. (2004). Wrightwood and the earthquake cycle: What a long recurrence record tells us about how faults work. *Geological Society of America Today*, *14*(9), 4. https://doi.org/10.1130/1052-5173(2004)014<4:WATECW>2.0.CO;2

Wells, D. L., & Coppersmith, K. J. (1994). New empirical relationships among magnitude, rupture length, rupture width, rupture area, and surface displacement. *Bulletin of the Seismological Society of America*, *84*(4), 974–1002.

Zechar, J. D., & Frankel, K. L. (2009). Incorporating and reporting uncertainties in fault slip rates. *Journal of Geophysical Research*, *114*(B12), B12407. https://doi.org/10.1029/2009JB006325

References From the Supporting Information

Chmeleff, J., von Blanckenburg, F., Kossert, K., & Jakob, D. (2010). Determination of the ^{10}Be half-life by multicollector ICP-MS and liquid scintillation counting. *Nuclear Instruments and Methods in Physics Research Section B: Beam Interactions with Materials and Atoms*, *268*(2), 192–199. https://doi.org/10.1016/j.nimb.2009.09.012

Lifton, N. (2016). Implications of two Holocene time-dependent geomagnetic models for cosmogenic nuclide production rate scaling. *Earth and Planetary Science Letters*, *433*, 257–268. https://doi.org/10.1016/j.epsl.2015.11.006

Lifton, N., Sato, T., & Dunai, T. J. (2014). Scaling in situ cosmogenic nuclide production rates using analytical approximations to atmospheric cosmic-ray fluxes. *Earth and Planetary Science Letters*, *386*, 149–160. https://doi.org/10.1016/j.epsl.2013.10.052